J. Fluid Mech. (1994), *vol.* 271, *pp.* 1–16

The turning couples on an elliptic particle settling in a vertical channel

By PETER Y. HUANG, JIMMY FENG AND DANIEL D. JOSEPH

Department of Aerospace Engineering and Mechanics, *and* The Minnesota Supercomputer Institute, University of Minnesota, Minneapolis, MN 55455, USA

(Received 26 April 1993 and in revised form 5 January 1994)

We do a direct two-dimensional finite-elment simulation of the Navier–Stokes equations and compute the forces which turn an ellipse settling in a vertical channel of viscous fluid in a regime in which the ellipse oscillates under the action of vortex shedding. Turning this way and that is induced by large and unequal values of negative pressure at the rear separation points which are here identified with the two points on the back face where the shear stress vanishes. The main restoring mechanism which turns the broadside of the ellipse perpendicular to the fall is the high pressure at the 'stagnation point' on the front face, as in potential flow, which is here identified with the one point on the front face where the shear stress vanishes.

1. Introduction

Joseph *et al.* (1987) and Fortes, Joseph & Lundgren (1987) discovered that the basic mechanisms controlling the motion and interactions of spherical bodies at moderate Reynolds numbers are associated with wakes and turning couples on long bodies. This was described by them as drafting, kissing and tumbling. Particles align in wakes and are sucked together. Kissing spheres aligned with the stream are unstable and tumble into arrangements in which the average orientation of lines between centres is across the stream. Hu, Joseph & Crochet (1992*a*) did a direct numerical simulation of unsteady two-dimensional solid–liquid two-phase flows using the Navier–Stokes equations for the liquid and Newton's equations of motion for the circular particles. Their numerical analysis reveals the effects of vortex shedding on the motion of the cylinders and reproduces the drafting, kissing, and tumbling scenario which is the dominant rearrangement mechanism in two-phase flow of solids and liquids in beds of large spheres that are constrained to move in only two dimensions. Hu, Joseph & Fortes (1992*b*) used the finite-element method to directly simulate the settling of an ellipse in a two-dimensional vertical channel. They constructed a video animation of the motion of the ellipse. The numerical results show that at moderately high Reynolds numbers, the particle rocks periodically in the channel. They tried to explain the turning mechanism by the high pressures at the front stagnation points as in potential flow. However, the pressure distribution on the particle surface in potential flow is not sufficient to explain the turning of the particles.

The settling of an ellipse in a viscous fluid is not a potential flow at the Reynolds number 60 used in the simulation. Wake effects are important; there is no pressure recovery and large negative pressures near the long ends of the ellipse where vortex shedding occurs can be even larger than the high pressures at the front. All these features appear in the simulation of Hu *et al.* (1992*b*), but the following questions not answered there are answered here: What is a 'stagnation point' in a viscous flow?

What is the distribution of shear stresses on the body of the ellipse? How are the separate torques per unit area of the surface due to pressure and to the shear stress distributed on the surface of the ellipse? What are the torque resultants? How does the pressure distribution on the back of the body control the rocking motion when there is vortex shedding?

In order to understand the driving and resisting forces on an ellipse settling and turning in a fluid, we calculate the stress distributions and the torque distributions on the particle surface. To do this, we had to enhance the numerical code used by Hu *et al.* (1992*a*) to compute torques due to pressures and viscous tractions. This is done in three steps. First we search for elements which have nodes on the particle surface and interpolate the velocity field to get the strain rate field in these elements. Then we set up a calculation procedure which gives the stress tensor on each node belonging to the particle surface. Finally the forces and torques on every segment of the surface can be evaluated and the total force and turning couple can be obtained.

We find that the torques due to the viscous shear stresses play an important role in resisting the turning of an ellipse but the dominant torques are due to three extreme values of the pressure which are here identified with negative pressures at two separation points on the back face and a positive pressure at a 'stagnation point' at the front face where the shear stress vanishes. Stagnation pressure always acts to put the broadside of the ellipse perpendicular to the fall, as in potential flow, but with the added caveats that in the viscous case the restoring mechanism acts only on the front face and the stagnation point is near the unique point at which the shear stress passes through zero. The negative pressure at the separation points sustains the periodic oscillation in both the particle position and its orientation.

2. Basic equations

Hu *et al.* (1992*a*), and Feng, Hu & Joseph (1994) have computed the velocity and pressure fields for the fluid caused by a settling elliptic particle in a vertical channel. The same procedure is used in our computation, which is briefly described in the following.

Consider a two-dimensional flow in an infinite vertical channel of width w. The fluid in the channel is assumed to be Newtonian and incompressible with density ρ_f and viscosity μ_f. Ω_t is the domain occupied by the fluid, Γ_t is its boundary. The velocity $\boldsymbol{u}(\boldsymbol{x}, t)$ and the pressure $p(\boldsymbol{x}, t)$ in the fluid are governed by the Navier–Stokes equations:

$$\left.\begin{aligned} \rho_f\left(\frac{\partial \boldsymbol{u}}{\partial t}+\boldsymbol{u}\cdot\boldsymbol{u}\right) &= \rho_f \boldsymbol{g}+\nabla\cdot\boldsymbol{\sigma} \\ \nabla\cdot\boldsymbol{u} &= 0 \end{aligned}\right\} \quad \text{on} \quad \Omega_t, \quad \forall t>0,$$

where $\boldsymbol{g}$ is the gravity vetor and $\boldsymbol{\sigma}$ is the stress tensor given by

$$\boldsymbol{\sigma} \overset{\text{def}}{=} -p\mathbf{1}+\boldsymbol{T} = -p\mathbf{1}+\mu_f[\nabla\boldsymbol{u}+(\nabla\boldsymbol{u})^T].$$

The velocity $\boldsymbol{u}$ satisfies no-slip conditions on the particle and at the walls of the channel.

The position of the solid elliptic particle sedimenting in the vertical channel can be determined by the coordinate of its centre $\boldsymbol{X} = (X, Y)$ and the turning angle α_p. The equation governing the motion of the particle is Newton's Law:

$$\left.\begin{aligned} m\frac{\mathrm{d}\boldsymbol{U}(t)}{\mathrm{d}t} &= \boldsymbol{F} \\ I\frac{\mathrm{d}\Omega(t)}{\mathrm{d}t} &= F_m \end{aligned}\right\} \forall t>0,$$

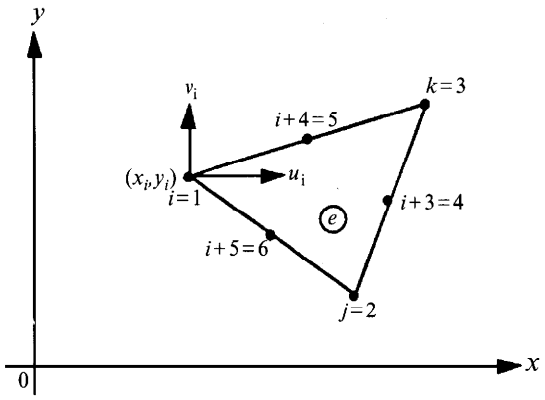

FIGURE 1. Triangle element e with three vertex nodes (i,j,k) and three midpoints.

where m is the mass of the elliptic particle and I is the moment of the inertia of the particle; $\boldsymbol{U}(t) = \mathrm{d}\boldsymbol{X}(t)/\mathrm{d}t$ is the velocity of the centre of the elliptic particle; $\Omega(t) = \mathrm{d}\alpha_p(t)/\mathrm{d}t$ is the angular velocity of the particle; $\boldsymbol{F}$ is the total force that the fluid exerts on the ellipse and F_m is the total torque around the centre of the ellipse.

The motion of the fluid and the motion of the solid elliptic particle are coupled. The fluid exerts forces and torques on the particle, thus changing the motion of the particle. At the same time, the motion of the solid elliptic particle induces flow by changing the position of the boundary and the velocities on the boundary.

Hu *et al.* (1992*a*) developed an explicit–implicit scheme to solve the motion of the elliptic particle. This scheme uses an explicit method to update the position of the particle and an implicit method to update the velocity of the particle. The updated position and velocity of the particle are used to update the boundary condition for the fluid equations. The nonlinear Navier–Stokes equations are solved by a finite-element package (POLYFLOW) which uses the Newton iterations to get the velocity and pressure distributions in fluid on the updated domain Ω_t subject to the updated boundary condition. The particle is then moved again by the explicit–implicit scheme and the procedure is repeated for the next time step.

In order to get the forces and torques exerted on the surface of the solid elliptic particle, Hu *et al.* (1992*a*) used a Gauss integral formula,

$$\int_{\Gamma_t} (\boldsymbol{\sigma}\cdot\boldsymbol{n})\cdot\boldsymbol{\omega}\,\mathrm{d}\Gamma = \int_{\Omega_t} \rho_f\left(\frac{\partial \boldsymbol{u}}{\partial t}+\boldsymbol{u}\cdot\nabla\boldsymbol{u}\right)\cdot\boldsymbol{\omega}\,\mathrm{d}\Omega + \int_{\Omega_t} \boldsymbol{\sigma}(p,\boldsymbol{u}):\nabla\boldsymbol{\omega}\,\mathrm{d}\Omega$$

where $\boldsymbol{\omega}$ is a vector-valued weighting function that is zero everywhere except on the boundary of the particle Γ. One can let $\boldsymbol{\omega} = \omega_1\boldsymbol{i}$ for computing F_x and $\boldsymbol{\omega} = \omega_2\boldsymbol{j}$ for computing F_y, where ω_1 and ω_2 are unity at the nodes on Γ and zero at any other nodes. By considering different weighting vectors ω in this way and using numerical integration, they obtained a force,

$$\boldsymbol{F} = F_x\boldsymbol{i}+F_y\boldsymbol{j} = \int_{\Gamma} \boldsymbol{\sigma}\cdot\boldsymbol{n}\,\mathrm{d}\Gamma,$$

acting on the solid particle. In the present paper we compute the forces and moments directly from the local velocity field. The numerical method is given in the next section.

3. Numerical analysis

We use the same governing equations for the motion of the fluid and the elliptic particle as those in Hu *et al.* (1992*a*). What we need to add now are direct calculations of the surface stresses and the torques due to pressure and viscous tractions. As the first step in the description of these procedures, we show how we interpolate the velocity in the elements which have at least one node lying on the surface of the particles. Then the strain rate tensor and stress tensor can be computed on the surface nodes.

3.1. *Interpolation of velocity*

Suppose that element e has at least one node on the particle surface. In figure 1, the velocity field inside the element can be approximated by second-order interpolation using the values of velocity $\boldsymbol{u}^e$ at the 6 nodes:

$$\boldsymbol{u}^e = (u, v) = \sum_{i=1}^{6} N_i(x, y)\, \boldsymbol{u}_i, \tag{1}$$

where the shape functions $N_i(x, y)$ are given as

$$\left.\begin{aligned} N_i(x,y) &= 2\lambda_i(\lambda_i - \tfrac{1}{2}), \\ N_{i+3}(x,y) &= 4\lambda_j \lambda_k, \end{aligned}\right\} \quad i = 1,2,3; \quad j = 2,3,1; \quad k = 3,2,1 \text{ respectively.}$$

Here λ_i are the area coordinates defined by

$$\lambda_i = \frac{a_i + b_i x + c_i y}{2\Delta^e}, \quad i = 1,2,3,$$

where

$$2\Delta^e = \det \begin{bmatrix} 1 & x_1 & y_1 \\ 1 & x_2 & y_2 \\ 1 & x_3 & y_3 \end{bmatrix},$$

$$\left.\begin{aligned} a_i &= x_j y_k - x_k y_j, \\ b_i &= y_j - y_k, \\ c_i &= x_k - x_j, \end{aligned}\right\}, \qquad i = 1,2,3; \quad j = 2,3,1; \quad k = 3,2,1 \text{ respectively.}$$

Let $\boldsymbol{N} = \begin{bmatrix} N_1 & 0 & N_2 & 0 & N_3 & 0 & N_4 & 0 & N_5 & 0 & N_6 & 0 \\ 0 & N_1 & 0 & N_2 & 0 & N_3 & 0 & N_4 & 0 & N_5 & 0 & N_6 \end{bmatrix}$, $\boldsymbol{U} = \begin{bmatrix} u \\ v \end{bmatrix}$

and $$\boldsymbol{V} = [u_1, v_1, u_2, v_2, u_3, v_3, u_4, v_4, u_5, v_5, u_6, v_6]^T;$$

then (1) can be expressed as

$$\boldsymbol{U} = \boldsymbol{N}\boldsymbol{V}. \tag{2}$$

3.2. *Stress tensor on a surface node*

The components of the strain-rate tensor are

$$D_{ij} = \frac{1}{2}\left[\frac{\partial u_i}{\partial x_j} + \frac{\partial u_j}{\partial x_i}\right],$$

so we can write

$$\boldsymbol{D} = \begin{bmatrix} D_{xx} \\ D_{yy} \\ D_{xy} \end{bmatrix} = \begin{bmatrix} \dfrac{\partial u}{\partial x} \\ \dfrac{\partial v}{\partial y} \\ \dfrac{1}{2}\left(\dfrac{\partial u}{\partial y} + \dfrac{\partial v}{\partial x}\right) \end{bmatrix} = \begin{bmatrix} \dfrac{\partial}{\partial x} & 0 \\ 0 & \dfrac{\partial}{\partial y} \\ \dfrac{1}{2}\dfrac{\partial}{\partial y} & \dfrac{1}{2}\dfrac{\partial}{\partial x} \end{bmatrix} \boldsymbol{U}$$

$$= \begin{bmatrix} \dfrac{\partial N_1}{\partial x} & 0 & \dfrac{\partial N_2}{\partial x} & 0 & \cdots & \dfrac{\partial N_6}{\partial x} & 0 \\ 0 & \dfrac{\partial N_1}{\partial y} & 0 & \dfrac{\partial N_2}{\partial y} & \cdots & 0 & \dfrac{\partial N_6}{\partial y} \\ \dfrac{1}{2}\dfrac{\partial N_1}{\partial y} & \dfrac{1}{2}\dfrac{\partial N_1}{\partial x} & \dfrac{1}{2}\dfrac{\partial N_2}{\partial y} & \dfrac{1}{2}\dfrac{\partial N_2}{\partial x} & \cdots & \dfrac{1}{2}\dfrac{\partial N_6}{\partial y} & \dfrac{1}{2}\dfrac{\partial N_6}{\partial x} \end{bmatrix} \boldsymbol{V}. \quad (3)$$

Then the strain-rate tensor for any position (x, y) in the element e is given by

$$D^e_{xx} = \frac{1}{2\Delta^e}[4(b_1 u_1 + b_2 u_6 + b_3 u_5)\lambda_1 + 4(b_1 u_6 + b_2 u_2 + b_3 u_4)\lambda_2 + 4(b_1 u_5 + b_2 u_4 + b_3 u_3)\lambda_3 - (b_1 u_1 + b_2 u_2 + b_3 u_3)], \quad (4a)$$

$$D^e_{yy} = \frac{1}{2\Delta^e}[4(c_1 v_1 + c_2 v_6 + c_3 v_5)\lambda_1 + 4(c_1 v_6 + c_2 v_2 + c_3 v_4)\lambda_2 + 4(c_1 v_5 + c_2 v_4 + c_3 v_3)\lambda_3 - (c_1 v_1 + c_2 v_2 + c_3 v_3)], \quad (4b)$$

$$D^e_{xy} = \frac{1}{4\Delta^e}[4(b_1 v_1 + b_2 v_6 + b_3 v_5 + c_1 u_1 + c_2 u_6 + c_3 u_5)\lambda_1 + 4(b_1 v_6 + b_2 v_2 + b_3 v_4 + c_1 u_6 + c_2 u_2 + c_3 u_4)\lambda_2 + 4(b_1 v_5 + b_2 v_4 + b_3 v_3 + c_1 u_5 + c_2 u_4 + c_3 u_3)\lambda_3 - (b_1 v_1 + b_2 v_2 + b_3 v_3 + c_1 u_1 + c_2 u_2 + {}_3 u_3)]. \quad (4c)$$

Suppose that there are N_k elements which share the same node k on the particle surface, as shown in figure 2. The strain-rate tensor in each element contributes to the velocity gradient at node k, and the arithmetic average from all N_k elements is taken as the velocity gradient at node k. We write the stress tensor for this node as

$$\boldsymbol{T} = \begin{bmatrix} \tau_{xx} & \tau_{xy} \\ \tau_{xy} & \tau_{yy} \end{bmatrix},$$

where the components are given by

$$[\tau_{xx}, \tau_{yy}, \tau_{xy}] = \frac{2\mu}{N_k} \sum_{e=1}^{N_k} [D^e_{xx}, D^e_{yy}, D^e_{xy}]. \quad (5)$$

3.3. *Pressure and stress torques on a particle surface*

After computing the stress tensor and pressure distribution at every node on the particle surface we can calculate the viscous part of the normal stress and the shear stress. The torques due to the pressure and the viscous stresses can then be obtained through the following steps.

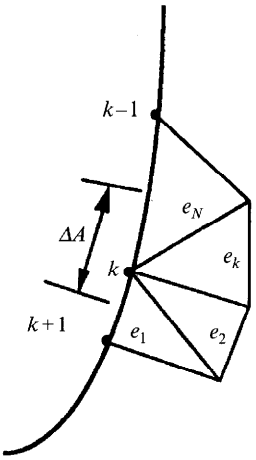

FIGURE 2. Particle surface node k and the N_k elements surrounding it.

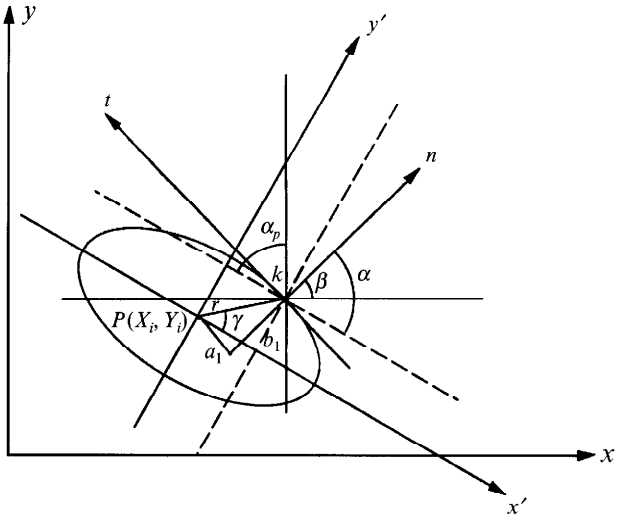

FIGURE 3. Coordinates of the surface of the ellipse. The x-axis is along the wall of the channel. $P(X_i, Y_i)$ is the centre of the ellipse and k is the node on the surface. α_p is the turning angle of the ellipse, $r = (x_k'^2 + y_k'^2)^{\frac{1}{2}}$ is the distance between node k and the center p. a_1 and b_1 are the arms of the forces F_n and F_t.

(i) In figure 3, the transformation of coordinates from x, y to x', y' is given by

$$\left.\begin{aligned} x' &= (x - X_i)\sin\alpha_p - (y - Y_i)\cos\alpha_p, \\ y' &= (x - X_i)\cos\alpha_p + (y - Y_i)\sin\alpha_p. \end{aligned}\right\} \tag{6}$$

(ii) In the x', y' system, the equation for the ellipse surface is

$$F(x', y') = \frac{x'^2}{a^2} + \frac{y'^2}{b^2} - 1 = 0$$

and the unit outer normal vector is $\boldsymbol{n} = \nabla F / |\nabla F|$.

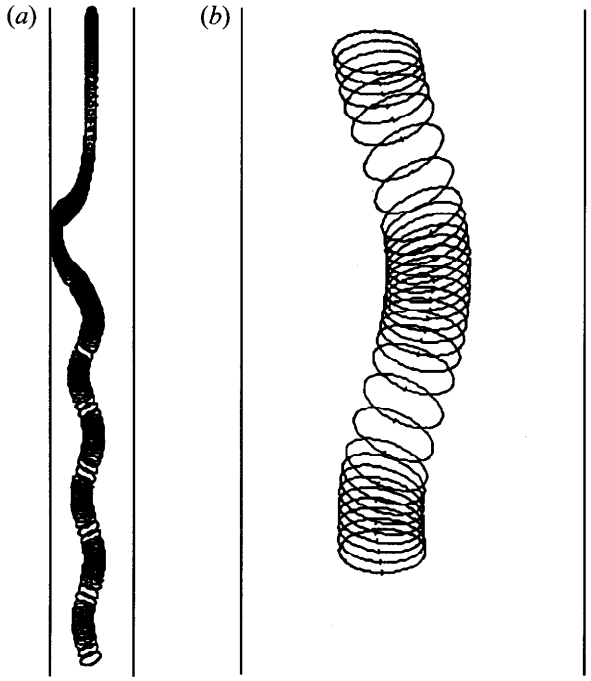

FIGURE 4. (*a*) Snapshots of the motion of the ellipse from rest to periodic oscillation. (*b*) Snapshots of the motion of the ellipse in one whole cycle. This cycle covers time steps from itime = 232 to 264.

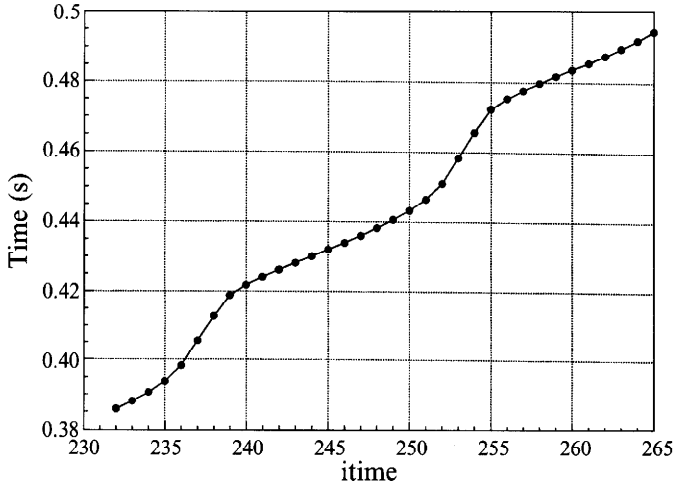

FIGURE 5. Real time at different time steps covered in one cycle of oscillation.

For a surface node k at (x'_k, y'_k), the unit normal vector $\boldsymbol{n} = (\cos\alpha, \sin\alpha)$ and the unit tangential vector $\boldsymbol{t} = (-\sin\alpha, \cos\alpha)$, where the angle α can be calculated by

$$\tan\alpha = \left(\frac{a}{b}\right)^2 \frac{y'_k}{x'_k}. \tag{7}$$

(iii) In the x, y system, the unit nornal vector is $\boldsymbol{n} = (\cos\beta, \sin\beta)$, the unit tangential vector is $\boldsymbol{t} = (-\sin\beta, \cos\beta)$, where $\beta = \alpha + \alpha_p - \frac{1}{2}\pi$.

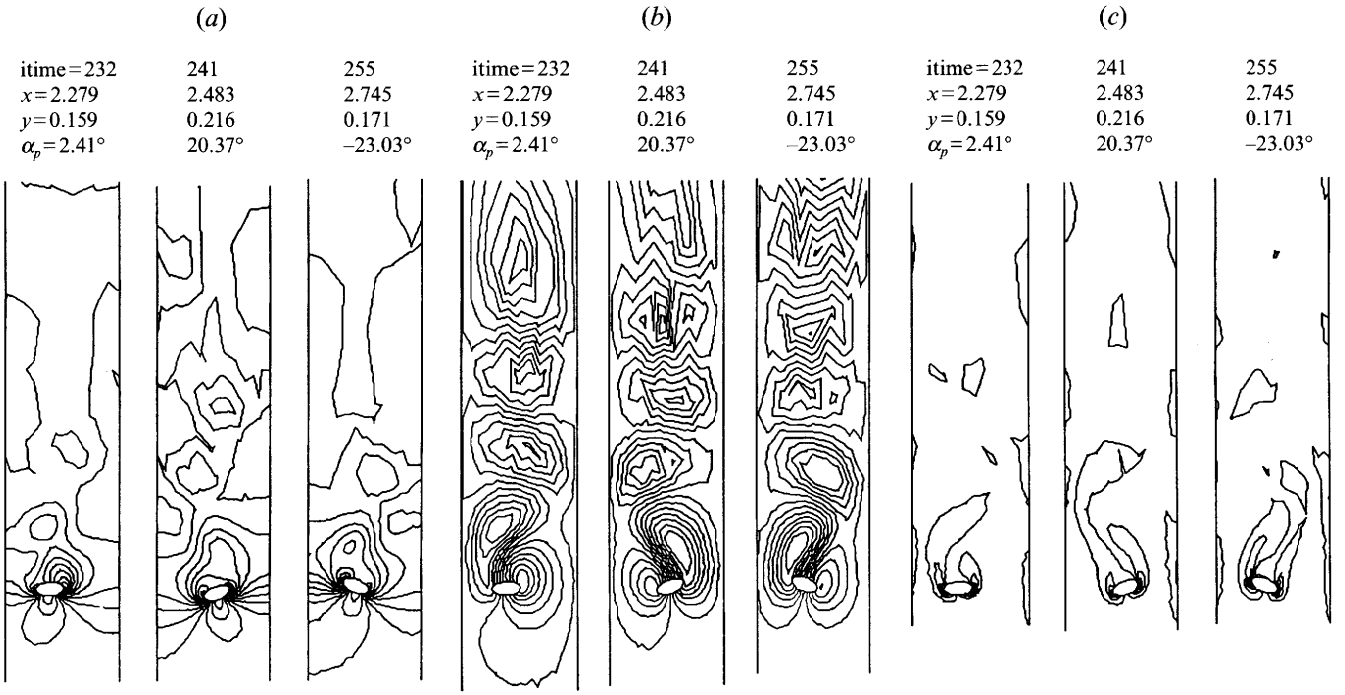

FIGURE 6. (*a*) Pressure contour for a sedimenting ellipse at three time steps. (*b*) Streamline contour plots for the sedimenting ellipse at three time steps. (*c*) Vorticity contour plots for the sedimenting ellipse in three different stages. (x, y, α_p) indicates the position of the ellipse.

(iv) The viscous force

$$\boldsymbol{F} = (\boldsymbol{n}\cdot\boldsymbol{T})\,\Delta A = (\cos\beta, \sin\beta)\begin{bmatrix}\tau_{xx} & \tau_{xy}\\ \tau_{xy} & \tau_{yy}\end{bmatrix}\Delta A,$$

where ΔA is the area of a region composed of one half of the two segments on both sides of node k:

$$\Delta A = \tfrac{1}{2}[(x_k - x_{k-1})^2 + (y_k - y_{k-1})^2]^{\frac{1}{2}} + \tfrac{1}{2}[(x_{k+1} - x_k)^2 + (y_{k+1} - y_k)^2]^{\frac{1}{2}}. \tag{8}$$

Here we assume constant pressure p and viscous stress tensor $\boldsymbol{T}$ in the region ΔA. The shear force then is given by

$$\begin{aligned} F_t = \boldsymbol{F}\cdot\boldsymbol{t} &= (\cos\beta, \sin\beta)\begin{bmatrix}\tau_{xx} & \tau_{xy}\\ \tau_{xy} & \tau_{yy}\end{bmatrix}\begin{bmatrix}-\sin\beta\\ \cos\beta\end{bmatrix}\Delta A \\ &= [-(\tau_{xx}\cos\beta + \tau_{xy}\sin\beta)\sin\beta + (\tau_{xy}\cos\beta + \tau_{yy}\sin\beta)\cos\beta]\,\Delta A. \end{aligned} \tag{9}$$

The normal stress $\tau_{nn} = \boldsymbol{n}\cdot\boldsymbol{T}\cdot\boldsymbol{n} = 0$ on the surface of a moving body. This can be readily seen by noting that on a rigid surface, the tangential gradient of the tangential velocity is zero, and by the no-slip condition and continuity, the normal gradient of the normal velocity in the fluid has to be zero.

(v) The pressure torque and viscosity torque can be calculated by

$$T_p = -pa_1\,\Delta A, \quad T_\tau = F_t b_1, \tag{10}$$

where

$$\left.\begin{aligned} a_1 &= r\sin(\alpha-\gamma) = x'_k\sin\alpha - y'_k\cos\alpha \\ b_1 &= r\cos(\alpha-\gamma) = y'_k\sin\alpha + x'_k\cos\alpha \end{aligned}\right\}. \tag{11}$$

4. Results and discussion

Our computations are based on the flow field (velocities and pressure) and particle motion simulated by the POLYFLOW code. The fluid is water, $\rho_f = 1.0$ g cm^{-1} and $\nu_f = 0.01$ cm^2 s^{-1}. The major axis of the ellipse is $a = 0.1$ cm; the ratio of major axis to minor axis is $k = a/b = 2$. The density of the solid particle is $\rho_s = 1.5$ g cm^{-3}. The width of the channel is $4a$. Initially the ellipse is at rest at the centre of the channel with its major axis parallel to the channel walls. It then starts to settle under gravity. The terminal mean sedimenting velocity is about $V = 5.6$ cm s^{-1} and the Reynolds number $Re = Va/\nu_f = 56$. The inflow boundary of the computational domain is placed $10a$ ahead of the ellipse and the outflow boundary is placed $15a$ behind of the ellipse. The surface of the ellipse is divided into 24 to 30 segments, the total number of nodes is between 2250 and 2500, depending on the computational domain. We computed 270 time steps. The ellipse's motion can be seen from the snapshots shown in figure 4(*a*). For the analysis of turning couples, we choose one cycle as in figure 4(*b*). The time interval Δt is determined by the computer at each time step, and figure 5 gives the correspondence between this time, which we denote 'itime', and the real time in the cycle shown in figure 4(*b*). The frequency of oscillation gives a Strouhal number $St = 0.187$, which is close to the value $St = 0.217$ at $Re = 155$ which we measured in an experiment in which a round cylinder with hemispherical ends oscillates as it falls in a water-filled sedimentation channel with close sidewalls. The experimental results will be reported in another publication. Contours of isobars, streamlines and iso-vorticity lines are shown in figures 6(*a*), 6(*b*) and 6(*c*) respectively.

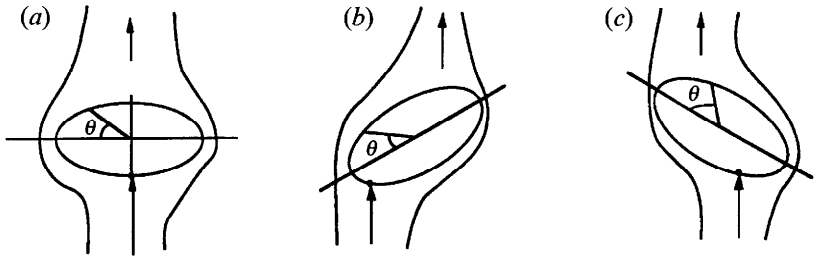

FIGURE 7. The shear stress vanishes at the stagnation points corresponding to dividing streamlines. (a) $\alpha_p = 0$: the ellipse is horizontal; (b) $\alpha_p > 0$: the ellipse tilts up on the right; (c) $\alpha_p < 0$: the ellipse tilts down on the right.

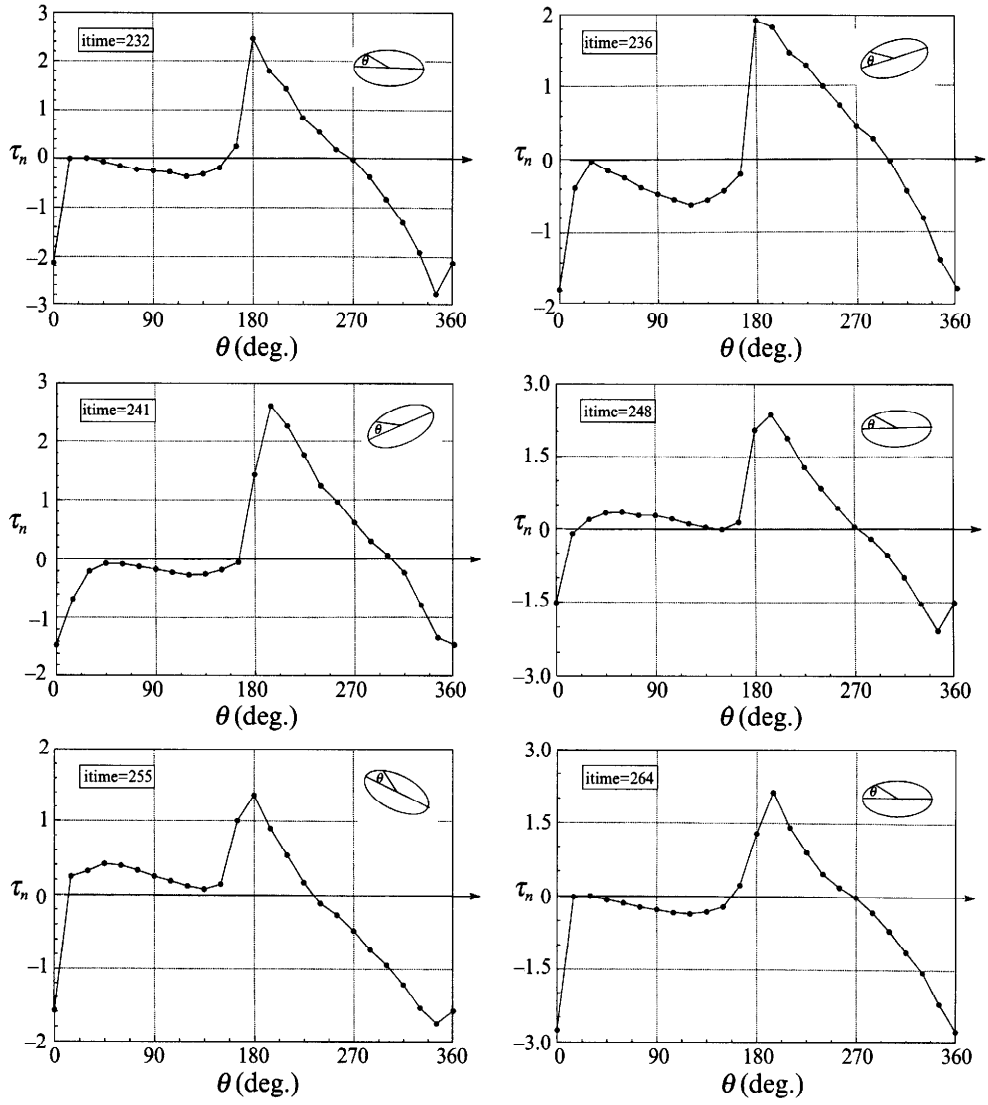

FIGURE 8. Shear-stress distribution on the ellipse for a motion cycle with time steps from itime = 232 to 264. The unit of the shear stress is dyne cm^{-2}.

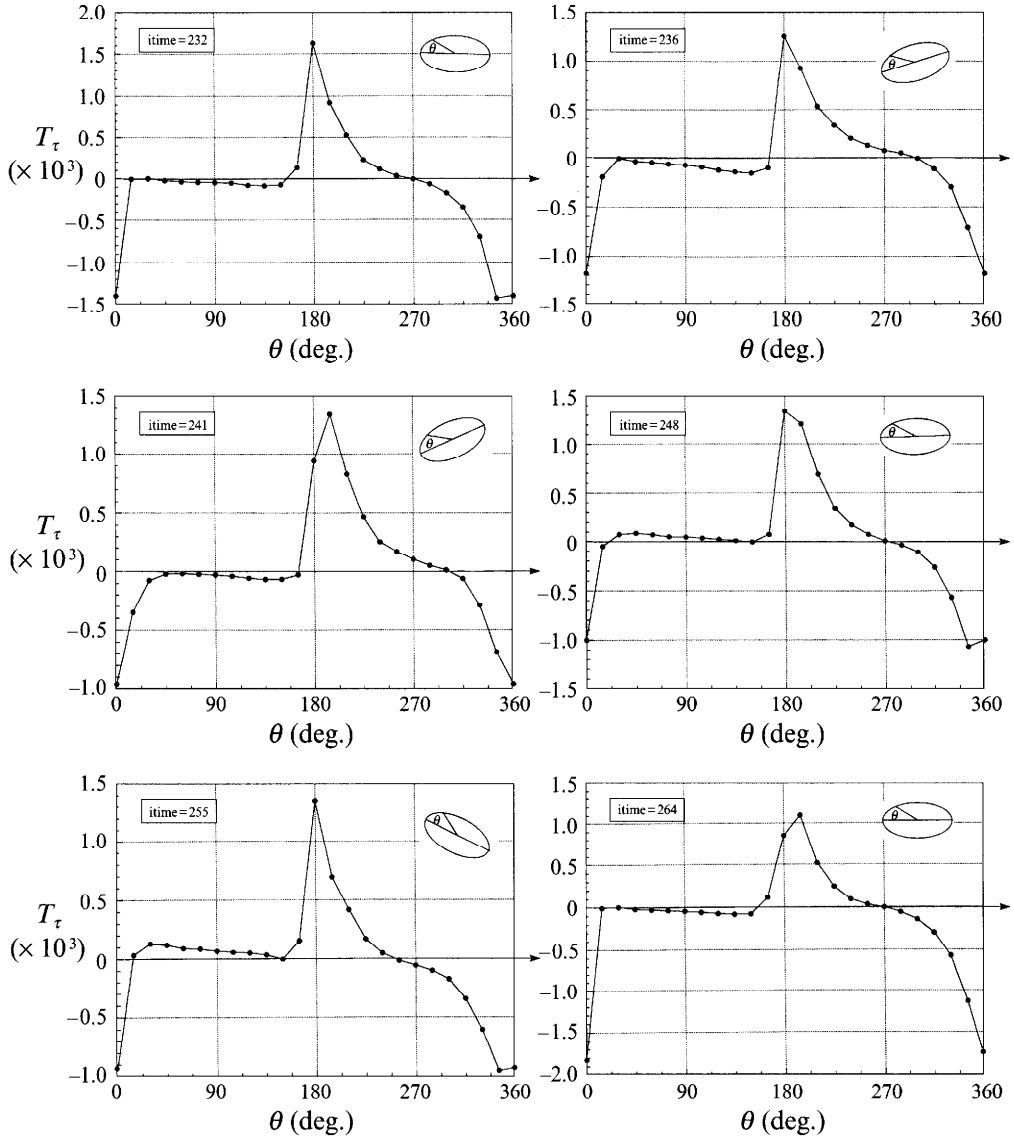

FIGURE 9. Torque distribution due to shearing on the ellipse for a motion cycle with time steps from itime = 232 to 264. The unit of the torque is dyne.

4.1. *Shear stress and position of stagnation and separation points*

In potential flows, the stagnation points are the points on the surface of the solid particle where the velocities of the fluid and the solid particle are the same. Since the fluid slips, all such points are on dividing streamlines. In viscous flow, this definition does not hold because the velocities of the fluid and the particle are the same at all points of the surface of the body. Therefore, we need a new definition for the viscous case. A little thought is required to convince oneself that 'stagnation points' ought to be the limits of dividing streamlines, a point of separation where the shear stress vanishes. We shall show that even in the viscous case, the pressure is nearly maximum at a point on the front face of the ellipse where the shear stress vanishes.

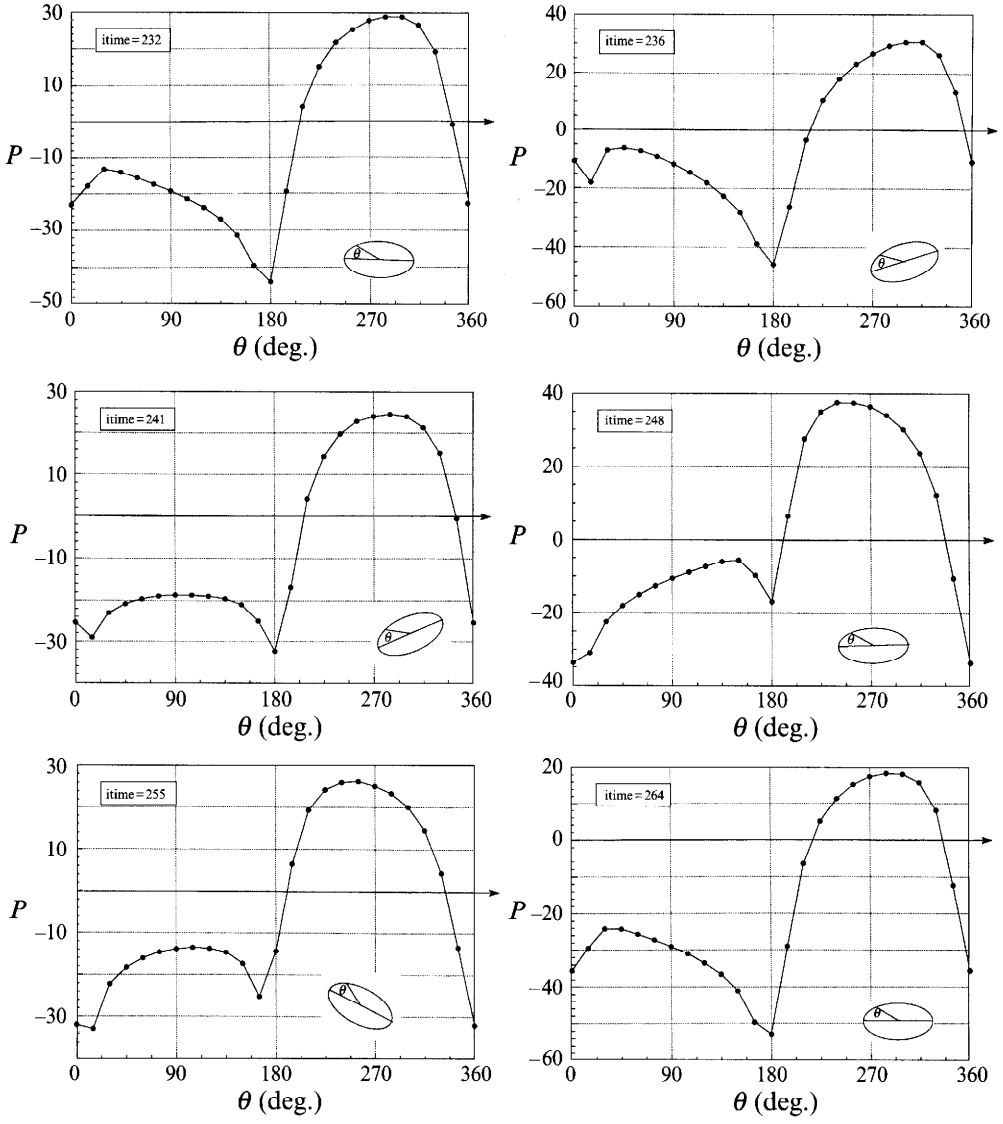

FIGURE 10. Pressure distribution on the ellipse for a motion cycle with time steps from itime = 232 to 264. The unit of the pressure is dyne cm^{-2}.

Figure 7 shows a cartoon of the ellipse in three different orientations and the position of the stagnation point on the forward face of the ellipse is clearly marked. The stagnation point is the place on the front face where the shear stress $\tau_n(\theta)$ goes through zero. In figure 8 we have plotted $\tau_n(\theta)$ for different times. The stagnation points oscillate about $\theta = 270°$. The other points at which $\tau_n(\theta)$ vanishes correspond to points of separation on the back of the ellipse. In figure 9 we have plotted the torque T_τ due to the shear stress. Naturally points at which τ_n vanishes have a vanishing contribution to the torque. The contributions of the shear stress to the torque are negative in the interval of θ between the front stagnation point and the first separation point (near $\theta = 0°$) on the back face.

The shear stresses arise from the translation and rotation of the ellipse. An important effect of viscosity is associated with the shedding of vortices at the back of

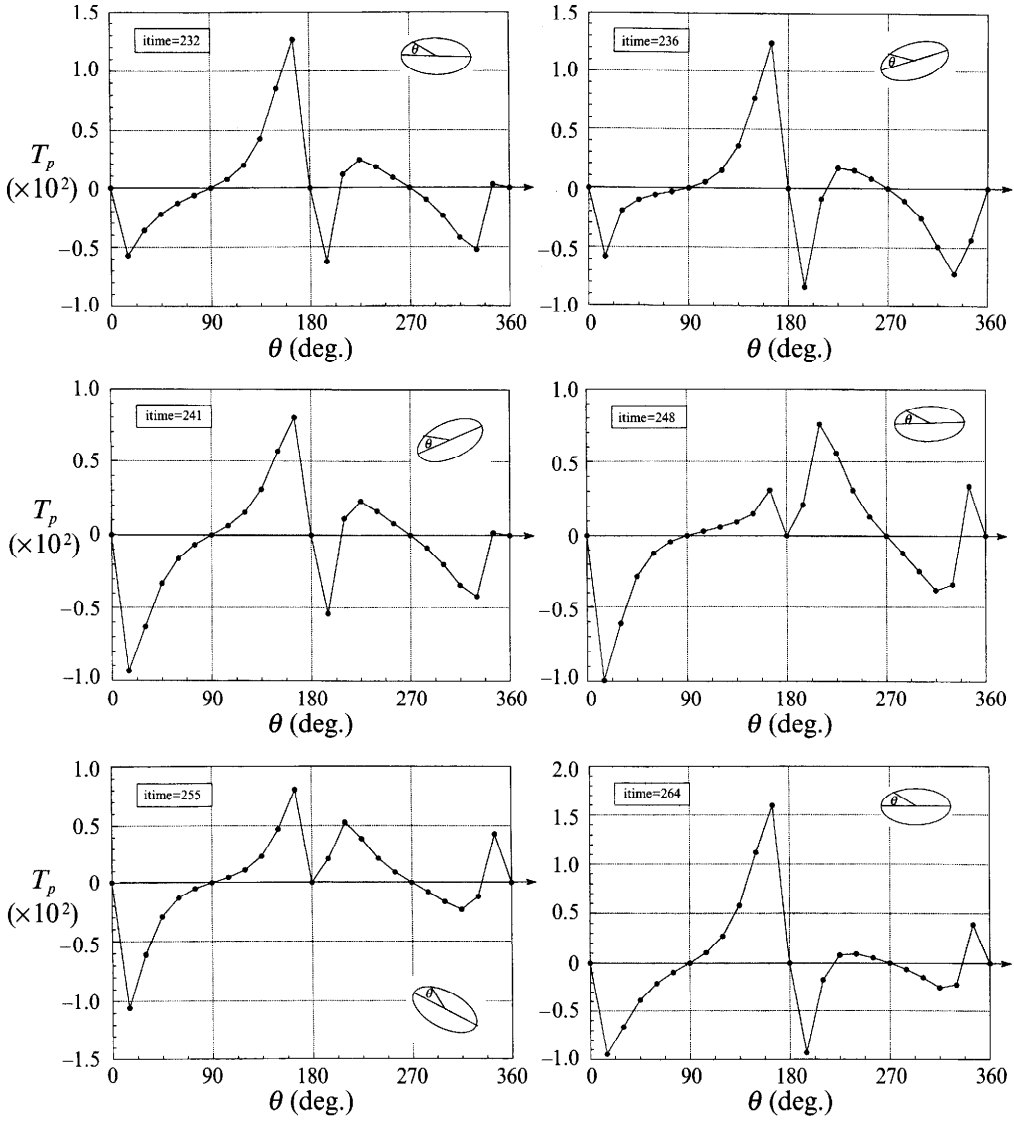

FIGURE 11. Pressure torque distribution on the ellipse surface for a motion cycle with time steps from itime = 232 to 264. The unit of the torque is dyne.

the ellipse. These shedding events are accompanied by high negative pressures which swing the ellipse periodically from side to side (figure 10). No matter how these negative pressures swing the ellipse, they are resisted from further turning by the stagnation pressure on the front side. The high negative pressures cannot dominate because they are relieved periodically by vortex shedding.

4.2. *Pressure*

Figure 10 shows the distribution of the pressure on the ellipse. The pressure is highest near the stagnation points where $\tau_n = 0$ (cf. figure 8). The pressure is positive on the front surface ($\theta = 180°$–$360°$) and negative on the rear surface ($\theta = 0°$–$180°$). The pressure distribution is asymmetric as a result of tilting and unsteady motion. From the diagrams we can see that the pressure distribution is asymmetric at itime = 232, 248,

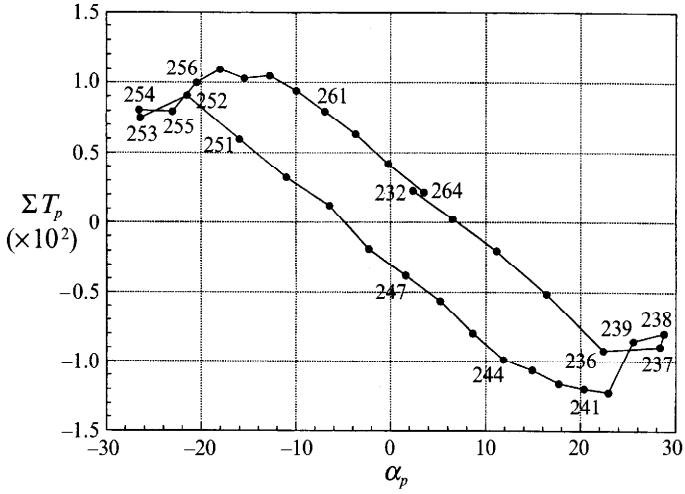

FIGURE 12. Total torque distribution due to pressure on the ellipse for a motion cycle with time steps from itime = 232 to 264. The unit of the torque is dyne.

264 although the ellipse is horizontal for those time steps, but at itime = 241 when the particle is tilted, the pressure distribution is somewhat symmetric.

The effect of vortex shedding is demonstrated to be the cause of the rocking motion. At itime = 232, a vortex is being discharged from the left back of the ellipse (figure 6*b*). This increases the pressure around $\theta = 0°$, and the unbalance between the negative pressures on the back surface of the ellipse at $\theta = 0°$ and $\theta = 180°$ turns the ellipse counter-clockwise, although the front stagnation pressure (at $\theta \approx 300°$) attempts to keep the major axis horizontal. At itime = 248, a vortex is being discharged from the right back of the ellipse, and this gives a higher pressure around $\theta = 180°$ which turns the ellipse clockwise, again against the will of the front stagnation pressure.

The torque distribution due to pressure is shown in figure 11. There are at least five points on the body where $T_p = 0$. On the four points $\theta = 0°$ (360°), 90°, 180°, 270°, the pressure points to the centre of the ellipse so that the moment arm is zero. On other points, the pressure goes to zero.

The total pressure torque ΣT_p varies periodically, and it is correlated to the orientation of the ellipse α_p as shown in figure 12. The difference in ΣT_p between time steps itime = 232 and 247 is the result of fluid inertia. In both cases, the major axis of the particle is roughly horizontal but the particle is turning in different directions. At itime = 237–239 and itime = 253–255, the ellipse has achieved the maximum tilt and the total pressure torque ΣT_p forces the ellipse to turn the other way, although there is some hesitation due to particle and fluid inertia. At itime = 237–239, $\Sigma T_p < 0$ and the pressure turns the ellipse clockwise. At itime = 253–255, $\Sigma T_p > 0$ and the pressure turns the ellipse counterclockwise. In conclusion, the pressure torque depends on the orientation of the particle and is always such as to turn the broadside of the ellipse perpendicular to the flow.

4.3. *Torque due to viscous tractions*

The total viscous torque ΣT_v can tell us in which direction the ellipse is turning. In figure 13, the value of the total viscous torque is basically correlated to the rotation of the ellipse. From time step itime = 239 to 253, the particle is turning clockwise (α_p decreasing) and the total viscous torque $\Sigma T_v > 0$ is in the counterclockwise direction.

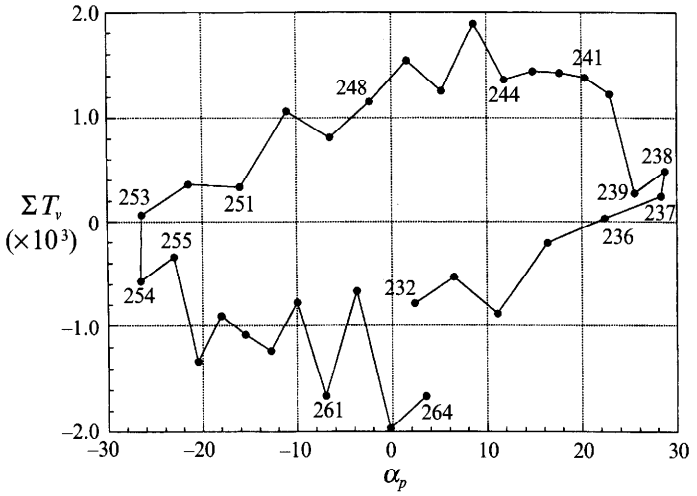

FIGURE 13. Total torque distribution due to viscosity on the ellipse for a motion cycle with time steps from itime = 232 to 264. The unit of the torque is dyne.

From time step itime = 254 to 264 and from itime = 232 to 237, the particle is turning counterclockwise (α_p increasing) and $\Sigma T_v < 0$ is in the clockwise direction. Therefore, viscous torque resists the turning of the ellipse most of the time. This is consistent with the intuition that the shear stress is caused by and counters the particle motion/rotation.

One can find, however, exceptions to this correlation. During time steps itime = 236, 237 and 238, the ellipse is attaining maximum tilt and its angular velocity is approaching zero (as a result of the front stagnation pressure). The fluid adjacent to the solid surface does not stop moving as readily because of inertia, and its motion gives rise to a positive viscous torque which is in the same direction as the rotation for a brief moment. Then the rotation reverses and the viscous torque again resists the rotation. A similar sequence of event exists between itime = 253 and 254.

Finally we note that the magnitude of the total viscous torque is about one order of magnitude smaller than the pressure torque, and therefore does not affect the principal features of the sedimentation.

5. Conclusion

Torques due to high pressures at the stagnation points (where the shear stress vanishes) on the front face of the ellipse always act to turn the broad side of the ellipse into the stream in a manner reminiscent of potential flow. Points of separation in the 'dead water' region on the back of the ellipse are the sites of vortex shedding which rocks the ellipse. Viscous torque caused by shear stress on the particle surface resists the motion, but does not alter the basic features of the motion determined by the high pressures at the stagnation and separation points.

Our work was supported by the NSF, fluid, particulate and hydraulic systems, by the US Army, Mathematics and AHPCRC, and by the DOE, Department of Basic Energy Sciences and the Minnesota Supercomputer Institute. We wish to thank Dr Howard Hu for help with the implementation and use of the code he developed, and for his comments and suggestions on the manuscript.

REFERENCES

FENG, J., HU, H. H. & JOSEPH, D. D. 1994 Direct simulation of initial value problems for the motion of solid bodies in a Newtonian fluid. Part 1. Sedimentation. *J. Fluid Mech.* **261**, 95–134.

FORTES, A. F., JOSEPH, D. D. & LUNDGREN, T. S. 1987 Nonlinear mechanics of fluidization of beds of spherical particles. *J. Fluid Mech.* **177**, 467–483.

JOSEPH, D. D., FORTES, A. F., LUNDGREN, T. S. & SINGH, P. 1987 Nonlinear mechanics of fluidization of beds of spheres, cylinders and disks in water. In *Advances in Multiphase Flow and Related Problems* (ed. G. Papanicolau), pp. 101–122. SIAM.

HU, H. H., JOSEPH, D. D. & CROCHET, M. J. 1992*a* Direct simulation of fluid particle motions. *Theoret. Comput. Fluid Dyn.* **3**, 285–306.

HU, H. H., JOSEPH, D. D. & FORTES, A. F. 1992*b* Experiments and direct simulations of fluid particle motion. *Intl Video J. Engng Res.* **2**, 17–24.